Correlation of stress and structure in a simple fluid confined to a pore with furrowed walls

D. J. Diestler*
Department of Agronomy, University of Nebraska–Lincoln, Lincoln, Nebraska 68583-0915

M. Schoen†
Iwan-N.-Stranski-Institut für Physikalische und Theoretische Chemie, Sekretariat ER1, Technische Universität Berlin, Straße des 17. Juni 112, D-10623 Berlin, Germany

(Received 17 May 2000)

A Lennard-Jones (12,6) film confined between two furrowed walls was simulated by the grand canonical ensemble Monte Carlo method. The walls are constructed by gouging triangular grooves in planar substrates that are structureless on the molecular scale. The furrows are infinitely long in one transverse direction (y) and of nanoscopic width (s_x) and depth (D). The furrows in the two walls are maintained parallel and in register. The diagonal components of the stress tensor ($T_{\alpha\alpha}$, $\alpha=x,y,z$) are computed as functions of D and the separation between the substrates (s_z) at fixed temperature, chemical potential, and s_x. The $T_{\alpha\alpha}$ for the film between the furrowed walls are strongly shifted from their counterparts for the film between flat (i.e., planar) walls. The shifts are rationalized in terms of the structure of the film, which becomes more ordered as the furrows deepen and the packing of film molecules becomes more restricted in the two dimensions normal to the y direction. The results demonstrate the profound impact of the coupling between molecular and nanoscopic scales on the properties of geometrically constrained fluids.

PACS number(s): 61.20.−p, 64.10.+h, 68.35.Rh, 68.45.Gd

I. INTRODUCTION

Unless solid surfaces are treated with extreme care, they are typically rough, so that an adjacent fluid is exposed to a geometrically disordered substrate. The effect of such disorder on wetting phenomena was studied experimentally [1–4] and theoretically [5–8] by coarse-grained approaches which average laterally over the height variation of the substrate. Thus an understanding of the *local* microscopic structure of fluids filling the grooves and covering the tips of such disordered substrates is still in its infancy. This dearth of information has been alleviated by the development of techniques for the fabrication of substrates with well defined geometrical structures periodic in one transverse dimension. One method utilizes the self-organization of vapor-deposited materials on crystalline substrates [9]. A recent example is the study by Rauscher *et al.* [10] of the confinement of organic molecules to one-dimensional trenches constructed by vapor deposition of CaF_2 on stepped (111) Si surfaces. A sequence of annealings produces a pattern of alternating CaF_2 and CaF stripes 1–16 nm wide. Adsorption of 3,10-dipropylperylene (DDP), followed by further annealing, results in DDP preferentially adsorbed on the CaF stripes. In nature one also encounters materials that are geometrically and chemically ordered on the nanoscale. For instance, minerals of the palygorskite and sepiolite group consist of stacks of alternating tetrahedral and octahedral silicate sheets [11].

Such structurally and chemically patterned substrates are envisioned to be useful in the field of ''microfluidics,'' which is concerned with the controlled movement of small quantities of valuable liquids across a substrate surface [12–16]. By imprinting substrates with nanoscopic chemical or geometrical patterns, one can modify the wetting characteristics of the underlying solid, thereby creating chemical ''lanes,'' say, along which a liquid can be transported from one region of the substrate to another, where it may subsequently be analyzed or undergo chemical reactions [15,16]. Thus it is conceivable that by imprinting a solid with different types of nanoscopic structures one may fabricate chemical chips or minute chemical factories [16].

Eventual realization of the controlled transport of fluids on the nanoscale by means of patterned substrates will be facilitated by fundamental studies of simple models for such systems [17]. It will be especially important to understand the phase behavior of such ''dimensionally constrained'' fluids. Indeed, a number of theoretical investigations were concerned with ''simple'' fluids (i.e., fluids comprising spherically symmetric molecules) adsorbed on chemically patterned substrates [18–24] and in pores with chemically patterned walls [25–32] (also see Refs. [33,34] for recent reviews). Applying a density-functional technique to the Lennard-Jones (LJ)(12,6) fluid confined between walls having a superimposed square-wave barrier, Chmiel *et al.* [25] found that pore condensation occurs in two stages: liquidlike bridges form first in the narrow gaps between the tops of the opposing barriers, followed by condensation in the wider gaps, so that the whole pore is eventually filled with liquid. This behavior is analogous to the two-stage filling process observed by Röcken and Tarazona [26] and Röcken *et al.* [27] in their lattice-gas [26] and density-functional [27] studies of adsorption of the LJ(12,6) fluid in a pore with a film-substrate potential varying sinusoidally in one transverse direction. Similar observations were made more recently in studies of the phase behavior of LJ(12,6) fluid confined to

*Electronic address: ddiestler1@unl.edu
†Electronic address: M.Schoen@physik.tu-berlin.de

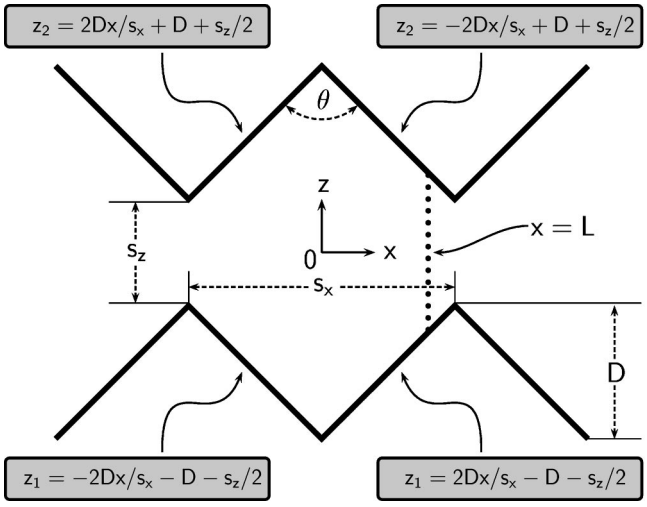

FIG. 1. Side view of a slit-pore with furrowed walls. Shadowed boxes display equations of planes of sides of ''central'' furrows. Subscripts 1 and 2 refer to lower and upper substrates, respectively.

slit pores with chemically striped walls [29–32]. By means of grand canonical ensemble Monte Carlo (GCEMC) simulations [29,30,32] and related mean-field lattice-gas models [30–32], particular emphasis is put on elucidating the interplay between different length scales set by the range of fluid-fluid interactions, confinement (i.e., width of the slit pore) and chemical decoration of the substrates (i.e., relative widths of the chemical stripes with which the substrates are endowed).

In this paper we are concerned with the properties of fluid films constrained by walls possessing purely structural patterns (as distinct from chemical patterns, which involve more than one chemical species) on the nanoscale. In an earlier work [35] we employed the GCEMC method to simulate the LJ(12,6) fluid between face-centered-cubic (100) walls, one smooth on the atomic scale and the other scored with square grooves several atomic diameters wide. When the walls are in the appropriate lateral alignment, the film consists of fluid and solid portions in thermodynamic equilibrium (fluid-filled grooves alternating with solid strips). Epitaxial freezing is induced by the templates of the strips between the grooves, an effect first described in Refs. [36] and [37]. In the grooves, however, the field due to the template is so weak that the film remains fluid there.

The current paper treats a LJ(12,6) fluid confined by substrates that are structurally striped on the nanoscale, but smooth on the *infinitesimal* scale. The substrate can be imagined to be constructed by gouging triangular grooves (furrows) in an infinitesimally smooth planar surface (see Fig. 1). In an earlier GCEMC study Schoen and Dietrich [38] examined the entropy-driven packing of hard spheres in the groove of a furrowed hard substrate. It was shown that under favorable conditions the furrow can induce a solidlike order of fourfold in-plane symmetry in the hard-sphere fluid [see Fig. 6(a) in Ref. [38]]. This observation was verified independently by Henderson *et al.* [39] in a density-functional calculation based on the Evans-Tarazona functional. More recently Rejmer *et al.* [40] studied the filling of a single furrow (wedge) by liquid. These authors employed an effective interface model, and focused on the meniscus of a (macroscopic) portion of fluid residing in the wedge. A similar approach was used by Parry *et al.*, who were concerned with wetting of a single furrow in $d=2$ [41] and $d=3$ dimensions [42]. Unlike Refs. [40–42] , the present work treats the fluid at the *molecular* scale. Further, in contrast to Refs. [38] and [39], here we take the intermolecular potentials to be continuous functions of the coordinates. We are primarily interested in the effects on thermophysical properties of coupling between the nanoscopic scale of the furrows and the molecular scale of the fluid structure. To attempt to elucidate these, we employ the GCEMC method to compute diagonal components of the stress tensor as functions of substrate separation s_z and dihedral angle θ associated with the furrow (see Fig. 1).

The remainder of this paper is organized as follows. In Sec. II we describe the model system. Section III is devoted to the derivation of statistical thermodynamic expressions for stress-tensor components. In Sec. IV we describe details of the computational methods. We present results in Sec. V, and conclude with a summary of our main findings in Sec. VI.

II. MODEL

Figure 1 displays a schematic of the model, which consists of a monatomic film constrained between two solid monatomic substrates that occupy the half spaces $s_z/2<z<\infty$ and $-s_z/2>z>-\infty$. The surface of each substrate is made up of plane segments perpendicular to the x-z plane, and so arranged as to create furrows extending from $y=-\infty$ to $y=\infty$. The substrates are therefore periodic in the x direction, having a period of s_x. They are also assumed to be infinite in the x direction. The dihedral angle θ between the sloping sides of a furrow is given in terms of the depth D of the furrow by

$$\theta = 2\arctan\left(\frac{s_x}{2D}\right). \tag{1}$$

We assume the furrows in the two substrates remain parallel in the y direction and in register in the x direction.

We take the potential energy to be expressible as a sum of LJ(12,6) interatomic potentials

$$u(r) = 4\epsilon\left[\left(\frac{\sigma}{r}\right)^{12} - \left(\frac{\sigma}{r}\right)^{6}\right] \tag{2}$$

between pairs of fluid molecules, where r is the distance between the pair. For simplicity, we assume all pairs are characterized by the same attractive well depth ϵ and effective diameter σ. To avoid complications that would attend specification of the detailed molecular structure of the substrate, we employ a mean-field approximation for the film-substrate potential energy, which is derived by averaging the (original) fluid-substrate interactions over the positions of the substrate atoms. Thus the mean-field potential energy $\Phi^{[2]}$ of a fluid molecule due to the *upper* substrate (designated by the superscript 2) is given by

$$\Phi^{[2]}(x,z) = \varphi_0^{[2]}(z) + \varphi_1^{[2]}(x,z), \tag{3}$$

where

$$\varphi_0^{[2]}(z)=\rho_s\int_{-\infty}^{\infty}dx'\int_{-\infty}^{\infty}dy'\int_{s_z/2+D}^{\infty}dz'\,u(|\boldsymbol{r}-\boldsymbol{r}'|),$$

$$\varphi_1^{[2]}(x,z)=\rho_s\sum_{m=-\infty}^{\infty}\int_{-\infty}^{\infty}dy'\int_{s_z/2}^{s_z/2+D}dz'\times\left[\int_{s_x(2m-1)/2}^{s_x[z'+D(2m-1)-s_z/2]/2D}dx'\,u(|\boldsymbol{r}-\boldsymbol{r}'|)+\int_{-s_x[z'-D(2m+1)-s_z/2]/2D}^{s_x(2m+1)/2}dx'\,u(|\boldsymbol{r}-\boldsymbol{r}'|)\right], \tag{4}$$

and ρ_s is the density of substrate atoms. The positions of fluid molecules and substrate atoms are $\boldsymbol{r}$ and $\boldsymbol{r}'$, respectively. The contributions $\varphi_1^{[2]}$ and $\varphi_0^{[2]}$ correspond to averages over the ''hills'' between the furrows and over the remainder of the substrate, respectively. Similar expressions obtain for the potential $\Phi^{[1]}$ of a fluid molecule due to the *lower* substrate (denoted by superscript 1).

Taking the origin at the fluid molecule and transforming to cylindrical coordinates, we can carry out the double integral in the first of Eqs. (4) to obtain

$$\varphi_0^{[2]}(z)=\frac{2\pi\epsilon\rho_s\sigma^3}{3}\left[\frac{2}{15}\left(\frac{\sigma}{s_2/2+D-z}\right)^9-\left(\frac{\sigma}{s_2/2+D-z}\right)^3\right]. \tag{5}$$

The definite integral on y' in the second of Eqs. (4) can also be done explicitly. The result is

$$\varphi_1^{[2]}(x,z)=\frac{3\pi\epsilon\rho_s\sigma}{2}\sum_{m=-\infty}^{\infty}\int_{s_z/2}^{s_z/2+D}dz'\times\left[\int_{s_x(2m-1)/2}^{s_x[z'+D(2m-1)-s_z/2]/2D}dx'\,\psi(x'',z'')+\int_{-s_x[z'-D(2m+1)-s_z/2]/2D}^{s_x(2m+1)/2}dx'\,\psi(x'',z'')\right] \tag{6}$$

where

$$\psi(x'',z'')=\frac{21}{32}\left(\frac{\sigma^2}{x''^2+z''^2}\right)^{11/2}-\left(\frac{\sigma^2}{x''^2+z''^2}\right)^{5/2}, \tag{7}$$

$x''=x-x'$, and $z''=z-z'$. Likewise, we can obtain the antiderivative of ψ with respect to x'' in closed form, but since the function of z' that results from evaluating it at the limits is formidably complex, we instead choose to calculate the double integral in Eq. (6) numerically (see Sec. IV). For this purpose it is convenient to recast $\varphi_1^{[2]}$ in dimensionless form as

$$\varphi_1^{[2]}(x,z)=\frac{3\pi\epsilon\rho_s\sigma s_x D}{4}\sum_{m=-\infty}^{\infty}\int_0^1 d\tilde{z}'\tilde{z}'\left[\int_0^1 d\tilde{x}'\,\psi(x'',z'')+\int_0^1 d\tilde{x}'\,\psi(\hat{x}'',z'')\right], \tag{8}$$

where

$$x''=x-\frac{s_x}{2}(\tilde{x}'\tilde{z}'+2m-1),$$

$$z''=z-D\tilde{z}'-\frac{s_z}{2}, \tag{9}$$

$$\hat{x}''=x-\frac{s_x}{2}(\tilde{x}'\tilde{z}'-\tilde{z}'+2m+1)$$

in terms of the dimensionless variables $\tilde{x}'$ and $\tilde{z}'$.

Since the total mean-field potential energy $\Phi=\Phi^{[1]}+\Phi^{[2]}$ is periodic in x, Φ need be calculated in only one period, say the ''central'' one $-s_x/2<x<s_x/2$ (see Fig. 1). Symmetry also dictates the following relations: $\Phi^{[1]}(x,z)=\Phi^{[2]}(x,-z)$ and $\Phi^{[k]}(x,z)=\Phi^{[k]}(-x,z)$, where $k=1$ and 2. From these latter we conclude that Φ at any point (x,z) in the central period is given by $\Phi(x,z)=\Phi^{[2]}(|x|,|z|)+\Phi^{[2]}(|x|,-|z|)$. We exploit this symmetry to simplify the computation of the fluid-substrate potential energy, as detailed in Sec. IV.

III. THERMOPHYSICAL PROPERTIES

A. Thermodynamics

From a thermodynamic perspective we take the *system* to consist of the finite portion of the fluid bounded by the substrate surfaces and by (imaginary) faces that lie in the pairs of planes $x=\pm s_x/2$ and $y=\pm s_y/2$. The thermodynamic state can be specified by giving the absolute temperature T, chemical potential μ, and spatial dimensions s_x, s_y, and s_z. In terms of these variables reversible transformations of the system can be expressed in differential form as

$$d\Omega=-\mathcal{S}dT-Nd\mu+F_x dL+F_y ds_y+F_z ds_z, \tag{10}$$

where Ω is the grand potential, $\mathcal{S}$ is the entropy, N is the number of film molecules, and L is an ancillary distance whose rôle is explained presently. The last three terms of Eq. (10) represent the mechanical work done by the system against forces applied to the faces. According to the assumptions thus far introduced, no shear stresses act on the system. The normal stress T_{zz} is given by

$$F_z=T_{zz}s_x s_y=\lim_{L\to s_x/2}\left(\frac{\partial\Omega}{\partial s_z}\right)_{T,\mu,L,s_y}, \tag{11}$$

where $s_x s_y$ is the cross-sectional area of the system in the x-y plane. Likewise the stress on the face pointing in the y direction is

$$F_y=T_{yy}s_x(s_z+D)=\lim_{L\to s_x/2}\left(\frac{\partial\Omega}{\partial s_y}\right)_{T,\mu,L,s_z}, \tag{12}$$

where $s_x(s_z+D)$ is the area of the face. The theoretical analysis of the expansion of the system in the x direction is complicated by the fact that the dimension of the system at which we wish to compute T_{xx} coincides with one of the variables (s_x) that determines the dihedral angle θ [see Eq. (1)]. To circumvent this problem, we introduce the auxiliary distance L (see Fig. 1). Thus we suppose that the face point-

ing in the x direction lies in the plane $x=L$, where $0\leqslant L \leqslant s_x/2$. Then we can write T_{xx} as

$$F_x = T_{xx}s_y s_z = \lim_{L\to s_x/2}\left(\frac{\partial\Omega}{\partial L}\right)_{T,\mu,s_y,s_z}. \tag{13}$$

B. Statistical mechanics

The connection between macroscopic and molecular levels is through the relationship [43]

$$\Omega = -k_B T \ln \Xi, \tag{14}$$

where the grand partition function is

$$\Xi = \sum_{N=0}^{\infty} \frac{\exp(\mu N/k_B T)}{N!\Lambda^{3N}} Z_N. \tag{15}$$

In Eq. (15), k_B is Boltzmann's constant, and Λ is the thermal de Broglie wavelength. The configuration integral is given by

$$Z_N = \prod_{i=1}^{N} \int_{-s_x/2}^{L} dx_i \int_{-s_y/2}^{s_y/2} dy_i \int_{z_1(x_i)}^{z_2(x_i)} dz_i \exp[-U/k_B T], \tag{16}$$

where the configurational energy is

$$U = \frac{1}{2}\sum_{i=1}^{N}\sum_{j=1\neq i}^{N} u(r_{ij}) + \sum_{i=1}^{N} \Phi(x_i, z_i). \tag{17}$$

Because the substrate surfaces are not parallel with the x-y plane, the limits on the integrations over the z coordinates in the expression for Z_N depend on the x coordinates; $z_1(x)$ and $z_2(x)$ are the equations of the planes of the lower and upper substrate surfaces, respectively (see Fig. 1).

From Eqs. (11)–(15) we deduce the statistical thermodynamic formula for the generic diagonal component of the stress tensor

$$T_{\alpha\alpha} = -\frac{k_B T}{\Xi A_\alpha}\sum_{N=0}^{\infty}\frac{\exp(\mu N/k_B T)}{N!\Lambda^{3N}}\left(\frac{\partial Z_N}{\partial s_\alpha}\right), \tag{18}$$

where s_α stands for the dimension of the system in the α direction, and A_α for the area of the face pointing in the α direction. The evaluation of $\partial Z_N/\partial s_\alpha$ is detailed in Appendix A.

Now substituting into Eq. (18) the successive intermediate expressions in Eqs. (A5), (A6), (A8), (A9), (A10), and (A11), we obtain

$$\begin{aligned} T_{xx} = &-\frac{k_B T}{V}\left[\langle N\rangle + \left\langle \sum_{i=1}^{N}\left(x_i+\frac{s_x}{2}\right)\frac{\Delta z'(x_i)}{\Delta z(x_i)}\right\rangle\right] \\ &+\frac{1}{2V}\left\langle \sum_{i=1}^{N}\sum_{j=1\neq i}^{N}\frac{u'(r_{ij})}{r_{ij}}\left\{x_{ij}^2 + z_{ij}\left[\frac{\Delta z'(x_i)}{\Delta z(x_i)}z_i\left(x_i+\frac{s_x}{2}\right)\right.\right.\right. \\ &\left.\left.\left.-\frac{\Delta z'(x_j)}{\Delta z(x_j)}z_j\left(x_j+\frac{s_x}{2}\right)\right]\right\}\right\rangle + \frac{1}{V}\left\langle \sum_{i=1}^{N}\frac{\partial\varphi_0}{\partial z_i}\right. \\ &\left.\times\left(x_i+\frac{s_x}{2}\right)z_i\frac{\Delta z'(x_i)}{\Delta z(x_i)}\right\rangle + \frac{1}{V}\left\langle \sum_{i=1}^{N}\left(x_i+\frac{s_x}{2}\right)\right. \\ &\left.\times\left[\frac{\partial\varphi_1}{\partial x_i}+\frac{\partial\varphi_1}{\partial z_i}z_i\frac{\Delta z'(x_i)}{\Delta z(x_i)}\right]\right\rangle \end{aligned} \tag{19}$$

where $\Delta z'(x_i)/\Delta z(x_i)$ is given by Eq. (A7), and $V \equiv s_x s_y s_z$. The angular brackets in Eq. (19) signify the grand canonical ensemble average, which is expressed for a generic dynamical quantity G by

$$\begin{aligned} \langle G\rangle &= \frac{1}{\Xi}\sum_{N=0}^{\infty}\frac{\exp(\mu N/k_B T)}{N!\Lambda^{3N}}\int_{\tilde{V}^N} d\boldsymbol{r}^N \exp[-U/k_B T]G(\boldsymbol{r}^N, N) \\ &= \sum_{N=0}^{\infty}\int_{\tilde{V}'^N} d\boldsymbol{r}'^N f_{eq}(\boldsymbol{r}'^N, N)G(\boldsymbol{r}'^N, N), \end{aligned} \tag{20}$$

where

$$f_{eq}(\boldsymbol{r}^N, N) = \frac{1}{\Xi}\exp(BN - \ln N!)\exp[-U(\boldsymbol{r}^N)/k_B T] \tag{21}$$

is the grand canonical ensemble probability density, and

$$B = \frac{\mu}{k_B T} - \ln\left(\frac{\Lambda^3}{\tilde{V}}\right) \tag{22}$$

is a dimensionless parameter which we introduce here for later convenience (see Sec. IV A). Note that in the second line of Eq. (20) the integration is over reduced coordinates $\boldsymbol{r}' = \boldsymbol{r}/V$. In Eq. (22), $\tilde{V} = s_x s_y (s_z + D)$ is the volume of the system (pore). In Eq. (19) the quantities $\partial\varphi_n^{[k]}/\partial\alpha_i$ ($n=0,1$, $k=1,2$, and $\alpha = x,z$) are just the negatives of the α components of the forces $f_{n,\alpha}^{[k]}(x_i, z_i)$ exerted by the substrates on fluid molecule i. Explicit expressions for these are presented in Appendix B.

By manipulations paralleling those used to reach Eq. (19) we find

$$T_{yy} = -\frac{1}{A_z(s_z+D)}\left[\langle N\rangle k_B T - \frac{1}{2}\left\langle \sum_{i=1}^{N}\sum_{j=1\neq i}^{N}\frac{u'(r_{ij})y_{ij}^2}{r_{ij}}\right\rangle\right] \tag{23}$$

and

$$\begin{aligned} T_{zz} = &-\frac{k_B T}{A_z}\left\langle \sum_{i=1}^{N}\frac{1}{\Delta z(x_i)}\right\rangle \\ &+\frac{1}{2A_z}\left\langle \sum_{i=1}^{N}\sum_{j=1\neq i}^{N}\frac{u'(r_{ij})z_{ij}}{r_{ij}}\left[\frac{z_i - z_1(x_i)}{\Delta z(x_i)}\right.\right. \\ &\left.\left.-\frac{z_j - z_1(x_j)}{\Delta z(x_j)}\right]\right\rangle + \frac{1}{A_z}\left\langle \sum_{i=1}^{N}\frac{\partial\Phi^{[2]}}{\partial z_i}\frac{z_i - z_2(x_i)}{\Delta z(x_i)}\right. \\ &\left.+\frac{\partial\Phi^{[1]}}{\partial z_i}\frac{z_i - z_1(x_i)}{\Delta z(x_i)}\right\rangle, \end{aligned} \tag{24}$$

where $A_z \equiv s_x s_y$ and z_1, z_2, and Δz are defined in Fig. 1 and Appendix A, respectively.

An alternative, much simpler, formula for T_{zz}, which can be derived by directly differentiating Z_N given in Eq. (16) (see Ref. [29] for details), is

$$T_{zz}=\frac{1}{2A_z}\left\langle \sum_{i=1}^{N}\left[\frac{\partial\Phi^{[2]}}{\partial z_i}-\frac{\partial\Phi^{[1]}}{\partial z_i}\right]\right\rangle=\frac{1}{2A_z}\left\langle \sum_{i=1}^{N}[f_z^{[1]}-f_z^{[2]}]\right\rangle, \tag{25}$$

where $f_z^{[k]}=f_{0,z}^{[k]}+f_{1,z}^{[k]}$ is the force on fluid molecule i due to substrate k. Equation (25) expresses the intuitive notion that the normal stress is just the mean force per unit area exerted on the fluid by the substrate.

C. Limits $D=0$ and $\epsilon=0$

In the limit $D=0$ ($\theta=180°$), when the substrates are planar, the following relations hold: $z_1=-s_z/2$, $z_2=s_z/2$, $\Delta z=s_z$, $\Delta z'=0$, and $\partial\varphi_1/\partial x=0$. Substituting these limiting relations into the expressions for the diagonal components of the stress tensor given in Eqs. (19), (23), and (24), we obtain

$$T_{\alpha\alpha}=-\frac{\langle N\rangle k_BT}{V}+\frac{1}{2V}\left\langle \sum_{i=1}^{N}\sum_{j=1\neq i}^{N}\frac{u'(r_{ij})\alpha_{ij}^2}{r_{ij}}\right\rangle,\quad \alpha=x,y \tag{26}$$

$$T_{zz}=-\frac{\langle N\rangle k_BT}{V}+\frac{1}{2V}\left\langle \sum_{i=1}^{N}\sum_{j=1\neq i}^{N}\frac{u'(r_{ij})z_{ij}^2}{r_{ij}}\right\rangle-\frac{1}{V}\left\langle \sum_{i=1}^{N}\left[f_z^{[2]}(x_i,z_i)\left(z_i-\frac{s_z}{2}\right)+f_z^{[1]}(x_i,z_i)\left(z_i+\frac{s_z}{2}\right)\right]\right\rangle.$$

These limiting formulas agree exactly with expressions previously derived for a slit–pore with planar walls (see Eqs. (26)–(32) in Ref. [29] for the special case $\epsilon_{fw}\equiv\epsilon_{fs}\equiv\epsilon_{ff}$).

Another limiting case is the one where $\epsilon\equiv0$ corresponding to the ideal-gas limit, in which intermolecular interactions become negligible and $T_{\alpha\alpha}$ should reduce to

$$T_{\alpha\alpha}=-\frac{\langle N\rangle k_BT}{\tilde{V}}, \tag{27}$$

where $\alpha=x,y,z$. Although T_{yy} given by Eq. (23) manifestly satisfies Eq. (27), it is hardly clear that T_{xx} and T_{zz} do so. We therefore investigate the particular case $\alpha\equiv x$. In the limit $\epsilon=0$, $U=0$, and the expression for T_{xx} given in Eq. (19) becomes

$$T_{xx}=-\frac{k_BT}{V}\left[\langle N\rangle+\left\langle \sum_{i=1}^{N}\left(x_i+\frac{s_x}{2}\right)\frac{\Delta z'(x_i)}{\Delta z(x_i)}\right\rangle\right]. \tag{28}$$

Using Eq. (20), we can write

$$\left\langle \sum_{i=1}^{N}\left(x_i+\frac{s_x}{2}\right)\frac{\Delta z'(x_i)}{\Delta z(x_i)}\right\rangle=\frac{1}{\Xi}\sum_{N=0}^{\infty}\frac{\exp(\mu N/k_BT)\tilde{V}^N}{N!\Lambda^{3N}}\times\left[\frac{1}{\tilde{V}}\sum_{k=1}^{N}\int_{\tilde{V}^N}d\boldsymbol{r}_k\times\left(x_k+\frac{s_x}{2}\right)\frac{\Delta z'(x_k)}{\Delta z(x_k)}\right]. \tag{29}$$

By means of Eqs. (A2) and (A7) the configuration integral in Eq. (29) can be evaluated explicitly:

$$\int_{\tilde{V}^N}d\boldsymbol{r}_k\left(x_k+\frac{s_x}{2}\right)\frac{\Delta z'(x_k)}{\Delta z(x_k)}=-Ds_xs_y. \tag{30}$$

Substitution of Eq. (30) into Eq. (29) yields

$$\left\langle \sum_{i=1}^{N}\left(x_i+\frac{s_x}{2}\right)\frac{\Delta z'(x_i)}{\Delta z(x_i)}\right\rangle=-\frac{Ds_xs_y\langle N\rangle}{\tilde{V}}. \tag{31}$$

Finally, combining Eqs. (28) and (31), we reach Eq. (27), with $\alpha\equiv x$. The demonstration for T_{zz} proceeds along a similar line.

IV. COMPUTATIONAL METHODS

A. Monte Carlo simulations in the grand canonical ensemble

To evaluate the ensemble averages in the formulas for $T_{\alpha\alpha}$, we employ the GCEMC algorithm originally proposed by Adams [44] (also see Ref. [45]), which consists of two consecutive sequences. In the first of these we select a fluid molecule, say i, from a given configuration $\boldsymbol{r}_m^{N_k}=\{\boldsymbol{r}_{1m},\boldsymbol{r}_{2m},\ldots,\boldsymbol{r}_{N_km}\}$ containing N_k molecules, and displace it at random according to

$$\boldsymbol{r}_{in}=\boldsymbol{r}_{im}+\delta(\mathbf{1}-2\boldsymbol{\xi}), \tag{32}$$

where $\boldsymbol{r}_{im}$ and $\boldsymbol{r}_{in}$ are the molecule's old and new positions, respectively, $\mathbf{1}=(1,1,1)$, δ is half the side length of a small cube centered on $\boldsymbol{r}_{im}$, and $\boldsymbol{\xi}$ is a vector whose three components are (pseudo) random numbers distributed uniformly on the interval $[0,1]$. The probability with which the displacement is realized is governed by $f_{eq}(\boldsymbol{r}^N,N)$ defined in Eq. (20), and must satisfy the *principle of detailed balance*. The latter is obeyed if the displacement is carried out as a Markov process [45]. The displacement must then be accepted with probability

$$\Pi_1=\min[1,\exp(-\Delta U_{nm}/k_BT)], \tag{33}$$

where $\Delta U_{nm}=U(\boldsymbol{r}_n^{N_k})-U(\boldsymbol{r}_m^{N_k})$ is the change in configurational energy associated with the process $\boldsymbol{r}_{im}\rightarrow\boldsymbol{r}_{in}$. During a run the magnitude of δ is adjusted such that roughly 40–60 % of all attempted displacements are accepted. The displacement sequence concludes once all N_k molecules have been considered consecutively. Since N_k remains fixed, this part of the GCEMC algorithm is equivalent to the classical Metropolis algorithm describing stochastic diffusion in configuration space [46] (see Ref. [47] for a historically interest-

ing discussion between M. N. Rosenbluth and J. G. Kirkwood concerning the correct implementation of the Metropolis algorithm).

In the second sequence of the GCEMC algorithm an attempt is made to alter the number of fluid molecules according to $N_n = N_m \pm 1$. The *principle of detailed balance* is again satisfied by carrying out the ''creation'' or ''destruction'' of a fluid molecule as a Markov process. Attempts to create and destroy fluid molecules are realized with equal probability. It can then be shown [45] that the change in the number of fluid molecules must be accepted with probability

$$\Pi_2 = \min[1, \exp(r_\pm)], \tag{34}$$

where

$$\exp(r_\pm) = \frac{f_{eq}(\boldsymbol{r}_n^{N_n}, N_n)}{f_{eq}(\boldsymbol{r}_m^{N_m}, N_m)},$$

$$r_+ = B - \ln N_n - \frac{U_{nm}}{k_B T}, \tag{35}$$

$$r_- = -B + \ln N_m + \frac{U_{nm}}{k_B T},$$

where ''+'' and ''−'' refer to creation and destruction, respectively, and $\Delta U_{nm} = U(\boldsymbol{r}_n^{N_n}) - U(\boldsymbol{r}_m^{N_m})$ because old and new (trial) configurations differ by one molecule. The probability of creation and destruction attempts is dictated solely by the thermodynamic state of the fluid, and cannot be adjusted as for displacement attempts. Employing scaled-particle theory, Allen determined the threshold of Π_2 at which the inefficiency of creation-destruction attempts causes the GCEMC algorithm to break down [48]. For the present thermodynamic state (see below), about 5×10^{-3} of all creation-destruction attempts are successful according to Eq. (34), which exceeds the minimum value of 10^{-4} given by Allen [48] by more than an order of magnitude. The creation-destruction sequence is repeated N_k^{init} times, where N_k^{init} is the number of fluid molecules present in the system when the creation-destruction sequence begins. The combination of N_k displacements and N_k^{init} creation-destruction attempts constitutes a ''Monte Carlo cycle.''

In the implementation of this algorithm a subtle complication arises because one is generally restricted to rather small systems on account of limited storage and computational speed. This implies that long-range intermolecular interactions such as the LJ(12,6) must be neglected during the simulation. Disregarding these interactions poses no problem to the calculation of ΔU_{nm} during the displacement sequence, since their contribution is small and cancels nearly exactly. However, this is not so for the creation-destruction sequence because of the shift in density of $\pm 1/\tilde{V}$ between old and new trial configurations. Nevertheless, the contribution of long-range interactions to ΔU_{nm} is still small. Thus one may resort to a mean-field treatment and estimate the long-range correction to ΔU_{nm} analytically [36]. Unfortunately, this approximation breaks down near the critical point of the confined fluid, where a mean-field treatment becomes inadequate [49]. To avoid these complications as well as the somewhat cumbrous expressions for corrections [36], we replace the LJ(12,6) potential [see Eq. (2)] in Eq. (17) by its shifted-force counterpart [50]

$$u(r) \to u_{sf}(r) = \begin{cases} u(r) - u(r_c) + du(r)/dr|_{r=r_c}(r_c - r), & r \leqslant r_c \\ 0, & r > r_c \end{cases} \tag{36}$$

which vanishes identically for all intermolecular distances exceeding the cutoff $r_c = 2.5\sigma$. The shifted-force potential is explicitly short range, and consequently does not require long-range corrections during the creation-destruction sequence of the GCEMC algorithm. However, we note in passing that the phase diagram of a fluid, in which intermolecular interactions are governed by u_{sf}, ineluctably depends on r_c.

B. Evaluation of fluid-substrate interaction potential

According to the discussion at the end of Sec. II, we compute $\varphi^{[2]}$ numerically at the nodes of a rectangular grid prior to the GCEMC run, and evaluate Φ by interpolation during the run. Following the constraints of symmetry summarized below Eq. (9), we evaluate $\varphi^{[2]}$ on a grid that covers the upper right quadrant of the x-z plane defined by the set of points $\{(x,z) | 0 < x < s_x/2, 0 < z < s_z/2 + D\}$ where, of course, $\varphi^{[2]} \equiv \infty$ if for a given x, $z \geqslant z_2(x)$ (see Fig. 1). The double integral in Eq. (8) is accomplished by repeated application of Simpson's rule. A mesh size of $1.25 \times 10^{-2}\sigma$ in both dimensions is fine enough to yield $\varphi^{[2]}$ with a precision of about 0.01%. Tests also reveal that terms in the sum in Eq. (8) are negligible for $|m| \geqslant 2$.

During the GCEMC run $\varphi^{[2]}(x_i, z_i)$, corresponding to the instantaneous position (x_i, z_i) of fluid molecule i, is found through bilinear interpolation. For this purpose we introduce dimensionless coordinates

$$\tilde{x}_i = \{[2x_i - (2n_x - 1)]\delta_x\}\frac{1}{2\delta_x},$$

$$\tilde{z}_i = \{[2z_i - (2n_z - 1)]\delta_z\}\frac{1}{2\delta_z}, \tag{37}$$

where $\{n_\alpha | n_\alpha \in \mathbb{N}, n_\alpha < \alpha_i/\delta_\alpha < n_\alpha + 1\}$ $(\alpha = x, z)$ and $\delta_x = \delta_z = 1.25 \times 10^{-2}\sigma$ is the mesh size. Defining weighting coefficients

$$w_{--} = (1 - \tilde{x}_i)(1 - \tilde{z}_i),$$

$$w_{-+} = (1 - \tilde{x}_i)(1 + \tilde{z}_i),$$

$$w_{+-} = (1 + \tilde{x}_i)(1 - \tilde{z}_i), \tag{38}$$

$$w_{++} = (1 + \tilde{x}_i)(1 + \tilde{z}_i),$$

we can express the interpolated value of $\varphi^{[2]}$ as

TABLE I. Normal component of the stress tensor T_{zz} from expressions given in Eqs. (24) and (25) for various furrow depths D and substrate separations s_z.

D	s_z	T_{zz} [Eq. (24)]	T_{zz} [Eq. (25)]
0.00	2.20	−0.232	−0.234
0.00	2.40	−2.479	−2.515
0.00	4.00	−0.659	−0.657
0.00	4.60	−1.146	−1.163
0.35	2.20	−1.760	−1.771
0.35	2.40	−1.513	−1.535
0.35	3.40	−1.155	−1.144
1.07	2.20	−1.258	−1.274
1.07	2.60	−1.096	−1.082
1.07	3.00	−1.002	−0.993
1.07	5.00	−0.986	−0.980
3.36	2.25	−1.059	−1.048
3.36	2.75	−0.984	−0.969

$$\varphi^{[2]}(x_i,z_i)\simeq\frac{1}{4}[w_{--}\Phi^{[2]}[n_x\delta_x,n_z\delta_z]+w_{-+}\Phi^{[2]}[n_x\delta_x,(n_z+1)\delta_z]+w_{+-}\Phi^{[2]}[(n_x+1)\delta_x,n_z\delta_z]+w_{++}\Phi^{[2]}[(n_x+1)\delta_x,(n_z+1)\delta_z]]. \tag{39}$$

Applying the bilinear interpolation method to the limiting case of planar substrates [where $\varphi^{[2]}(x,z)$ can be evaluated by the explicit expression for $\varphi_0^{[2]}$ in Eq. (5)], we verified that the interpolated value of $\varphi^{[2]}(x,z)$ at any point in the x-z plane deviates by less than 0.1% from the value calculated from Eq. (5).

V. RESULTS AND DISCUSSION

In the remainder of this paper we express all quantities in the customary dimensionless (i.e., ''reduced'') units. That is, length, energy, stress, and temperature are expressed in units of σ, ϵ, ϵ/σ^3, and ϵ/k_B, respectively. For all thermodynamic states of the system considered, $T=1.0$ and $\mu=-9.0$; the corresponding bulk density and pressure are $n_b=0.709$ and $P_b=0.979$, respectively. The width of the furrow is fixed at $s_x=8.0$; the length of the furrow is chosen in the range $8.0\leqslant s_y\leqslant 40.0$. The cutoff radius is set to $r_c=2.5$. The depth of the furrow D (or equivalently the dihedral angle θ) and the separation s_z were varied more or less systematically as described below. The results are based upon runs of 5×10^4 Monte Carlo cycles; each run is started from a random configuration of fluid molecules.

To demonstrate the reliability of the GCEMC procedure, we compare the components of T_{zz} computed from the dissimilar expressions given in Eqs. (24) and (25). The entries in Table I for a number of arbitrarily selected cases agree to better than 2%, supporting the internal consistency of the simulations.

Figure 2 displays plots of $T_{\alpha\alpha}$ ($\alpha=x,y,z$) versus s_z for several fixed values of θ. For the case $\theta=180°$, T_{zz} versus s_z is the normal-stress curve for the planar, smooth-wall slit pore; T_{xx} and T_{yy} are related to the interfacial tension γ by $\gamma=[(T_{xx}+T_{yy})/2-T_{zz}]$. The oscillations correspond to the abrupt appearance of successive layers in the film as s_z increases [45]. For the particular thermodynamic state under consideration (see above), at $s_z=2.0$ the film consists of a single layer parallel to the substrate surfaces. The layer is homogeneous and isotropic in transverse directions (i.e., the x and y directions parallel with the substrate surfaces) and inhomogeneous in the normal direction (i.e., the z direction). The film molecules are close packed in the layer, which fits snugly between the substrates. Indeed the film is under a slight tension in the z direction, that is $T_{zz}>0$ and an outward force $T_{zz}s_xs_y$ must be applied to the substrates in order to maintain the separation fixed at $s_z=2.0$. Now, as s_z increases from 2.0, more fluid molecules enter the pore and disrupt the close packing of the monolayer. Consequently, T_{zz} drops precipitously, reaching a minimum about $s_z=2.5$ [see Figs. 2(c) and 2(d)]. As s_z continues to increase, however, the original monolayer begins to split, resulting eventually in two close-packed layers at $s_z=3.0$, where T_{zz} reaches a relative maximum. The completion of the new layer, with the attendant increase in order (with respect to the intermediate state of the partially formed layer), drives the system toward a state of tension (with respect to the bulk phase) in the z direction. This cycle repeats as s_z increases from 3.0 to 4.0, where three layers of fluid are present under tension (relative to the bulk phase) in the z direction.

We now adapt the above ideas relating structure and tension in order to rationalize the dependence of $T_{\alpha\alpha}$ on D with s_z fixed, which is shown in Fig. 3. We consider T_{zz} first. At $D=0.0$ ($\theta=180°$), which corresponds to the planar limit, the values of T_{zz} are just the relative maxima at $s_z=2.0$, 3.0, and 4.0, respectively [see Figs. 2(c) and 2(d)], where one-, two-, and three-layer films are present. We focus now on the monolayer fluid. As D increases, that is as the furrow deepens, the original monolayer is disrupted, which results in a sharp decline in T_{zz}, analogous to that observed as the distance s_z between the planar substrates increases from $s_z=2.0$, as described above. However, when D increases, the effective distance d between the substrate surfaces increases nonuniformly from the edges of the furrow at $x=\pm s_x/2$ to the center at $x=0$. That is, at the edges $d_e=s_z$, whereas at the center $d_c=s_z+2D$. Hence the degree of disorder varies over the furrow, being least at the edges and greatest near the middle.

At $\theta=170°$, T_{zz} has reached a (relative) minimum. From Eq. (1) we compute $D=0.35$, so that $d_c\simeq2.7$. Judging from the above discussion of the planar limit, one might surmise that the original monolayer should be splitting into two layers over the central region of the furrow. Another factor comes into play, however, to enhance the ordering of the film near the vertex of the furrow: the substrate surfaces now intersect in a line (vertex) to create a ''corner'' with respect to which atoms can order themselves in the direction parallel with the substrate surface and normal to the y axis. As a measure of the order of the fluid we take the local density, which can be expressed

$$\rho(x,z)=\frac{\langle N(x,z)\rangle}{\Delta x\Delta z s_y}, \tag{40}$$

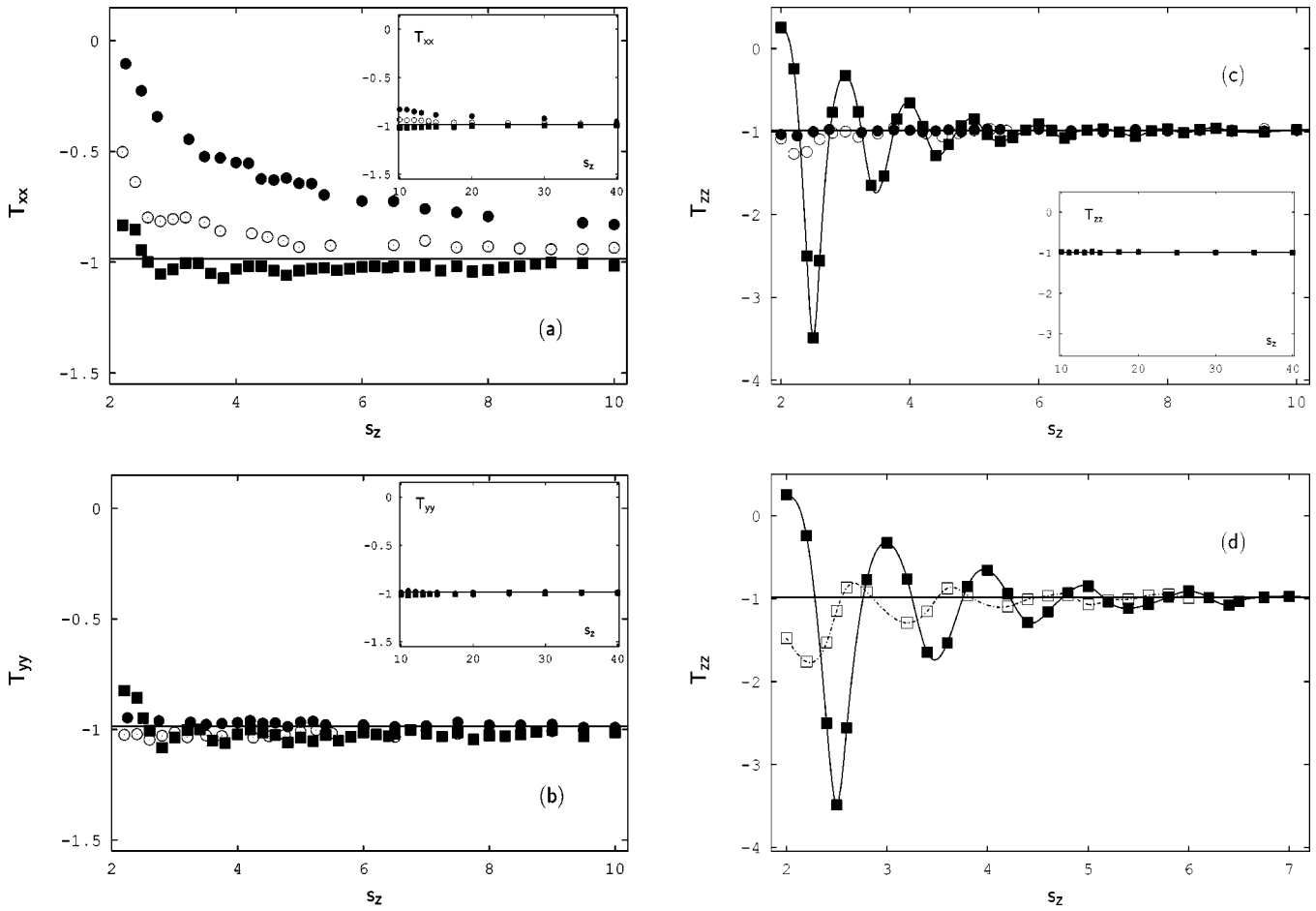

FIG. 2. Diagonal components ($T_{\alpha\alpha}$, $\alpha=x,y,z$) of the stress tensor as functions of separation s_z for several furrow depths D. Panels (a), (b), and (c): (■), $D=0.00$ ($\theta=180°$); (○), $D=1.07$ ($\theta=150°$); (●), $D=3.36$ ($\theta=100°$). Panel (d): (■), $D=0.00$ ($\theta=180°$); (□), $D=0.35$ ($\theta=170°$). The solid horizontal line represents $-P_b=-0.979$.

where $\langle N(x,z)\rangle$ stands for the ensemble-average number of fluid molecules that lie within a square prism of dimensions $\Delta x\times\Delta z\times s_y$ centered on the node of the grid at the point (x,z). The plot of ρ in Fig. 4(b) indicates that the monolayer film has indeed bifurcated into quite sharp layers near the center of the pore. These merge into a single layer near the edges. As a result the normal stress drops to an intermediate value between the limiting (planar) values of 0.25 at $s_z=2.0$ and -1.8 at $s_z=2.7$.

As θ continues to decrease, the furrow becomes deeper and the corner sharper. The consequence is an increasingly ordered fluid in both transverse dimensions. The furrow can be viewed as being spanned in the z direction by segments of fluid containing integral numbers of layers, alternating with segments ''in transit'' (that is, segments in which new layers are coming into being). Therefore, T_{zz} oscillates as D increases to about 1.66 ($\theta=135°$). For larger D, the broad midsection of the pore is dominated by large (asymptotic) separations, and hence T_{zz} is near the bulk stress. The structure of T_{zz} versus D for the cases $s_z=3.0$ and 4.0 [see Fig. 3(c)] may be similarly rationalized. As expected, the oscillations become muted as s_z increases and T_{zz} approaches the asymptotic (large s_z) value more rapidly.

The dependence of T_{zz} on s_z for fixed D is shown in greater detail in Fig. 2(d). The normal stress curve for the furrowed substrate appears to be shifted and dampened with respect to the limiting curve for the planar substrate. This can be explained crudely as follows. The segments of the film that span the pore in the z direction consist of different numbers of layers in the process of forming. Roughly speaking, the normal stress can be expressed as a weighted average over the segments of the limiting stress for planar substrates at a separation that corresponds to the distance between the sloping substrate surfaces for that segment. If D is not too far from 0.0 ($\theta=180°$), then the average involves only a few points on the limiting stress curve, which are separated from one another by fixed distances as s_z changes. Thus, we expect the average to have the same period as the limiting curve, but also to be dampened through partial cancellation. The plots in Fig. 2(d) bear this out. As D becomes larger, the average involves a larger number of segments and a correspondingly larger number of points on the limiting curve. A sufficiently deep furrow, say, $D=3.37$ ($\theta\approx100°$) [see Fig. 2(c)], results in essentially complete cancellation.

We turn now to an examination of the dependence of T_{xx} on D for fixed s_z. For the case $s_z=2.0$, Fig. 3(a) shows that the film tends more or less linearly with increasing D toward a state of tension in the x-direction. The plots of local density in Fig. 4 suggest that the film becomes more ordered in both the x and z directions as D increases. Further evidence that order in the film increases as the furrow deepens is provided by a plot of mean density

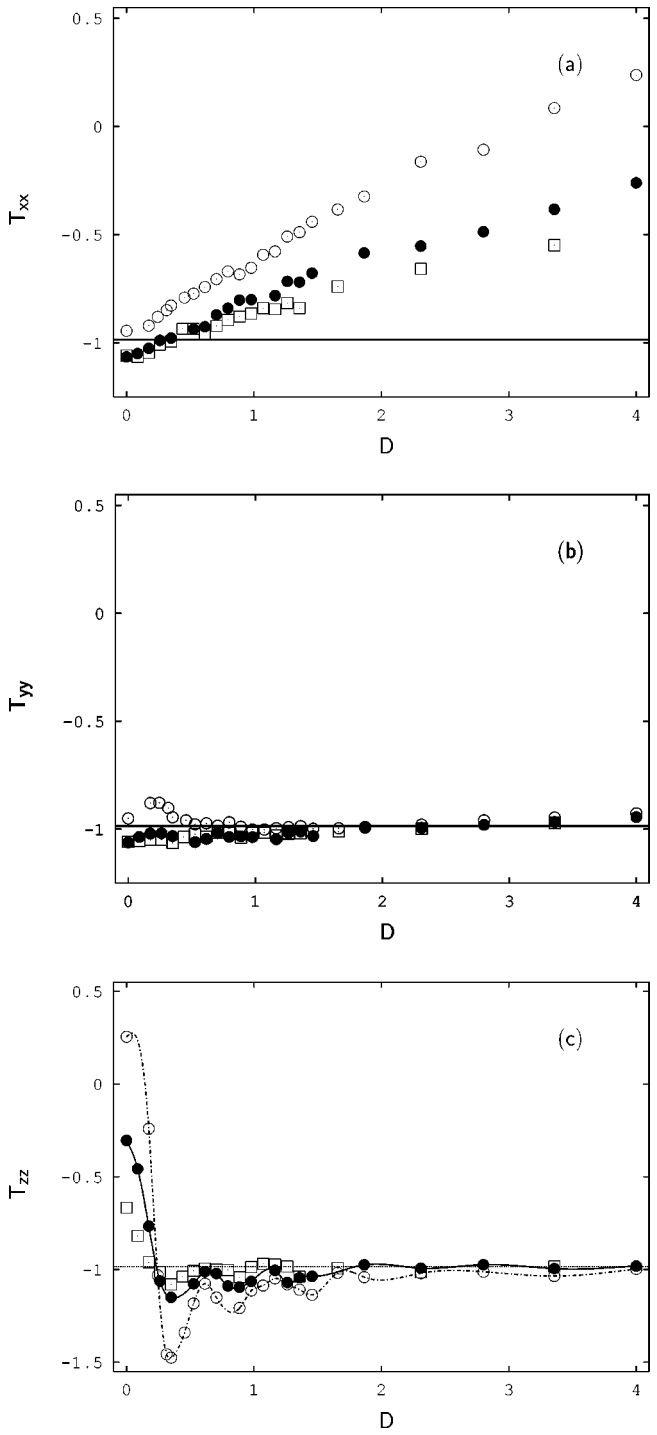

FIG. 3. Diagonal components ($T_{\alpha\alpha}$, $\alpha=x,y,z$) of the stress tensor as functions of furrow depth D for several substrate separations $s_z=2.0$ (○), 3.0 (●), and 4.0 (□). Solid horizontal line represents $-P_b=-0.979$.

$$n=\frac{1}{Ds_x+s_xs_z}\left[\int_{-s_x/2}^{0}dx\int_{z_1(x)}^{z_2(x)}dz\rho(x,z)+\int_{0}^{s_x/2}dx\int_{z_1(x)}^{z_2(x)}dz\rho(x,z)\right]=\frac{\langle N\rangle}{\tilde{V}} \tag{41}$$

as a function of D (Fig. 5). That n increases monotonically with D indicates that the efficiency of packing of fluid molecules increases accordingly. Further, as one would expect, both the amount of increase in n and rate of increase of n (i.e., dn/dD) are smaller the greater s_z is. When $s_z=2.0$ the film is forced to be monolayer near the edges. As the furrow deepens and the corner sharpens, the order in the layer nearest the substrate surface (i.e., the contact layer) increases in the direction parallel with the substrate surface and with the x-z plane. This increase in order is conferred on the x direction through a ''template effect.'' That is, the contact layer provides a template to which the next layer conforms. This epitaxial effect persists for a few layers. Thus the film proceeds toward a condition of higher tension (relative to the bulk phase) in the x direction, for the same reason that the film between planar substrates tends to a state of higher tension in the z direction as a new layer is completed and the order increases to a ''local'' maximum. Likewise, with increasing s_z the effect just described is muted [see Fig. 3(a)]. As s_z increases, the fraction of the x directed face that is covered by the disordered asymptotic (large s_z) region increases.

The dependence of T_{yy} on D at fixed s_z is markedly weaker than that of T_{xx} or T_{zz} on D at fixed s_z [see Fig. 3(b)]. The reason is that T_{yy} is associated with expansion (compression) in the y direction, in which the degree of order does not change as D or s_z is altered. Nevertheless, T_{yy} depends on structural variations of the fluid in the x and z directions (i.e., variations parallel with the cross section of the pore). The case $D=0.0$ illustrates this clearly. As the plots in Fig. 2(b) show, T_{yy} oscillates with increasing s_z, in correspondence with the appearance of successive layers of fluid, as described in connection with the s_z dependence of T_{zz}. The variations of T_{yy} with s_z are strongest in the vicinity of $D=0.0$. When D is sufficiently small that the cross section of the pore is dominated by the asymptotic (large s_z) regime, then T_{yy} approaches the bulk stress. Again, the larger s_z is, the weaker is the dependence of T_{yy} on D [Fig. 2(b)].

VI. CONCLUSIONS

The results presented in Sec. V demonstrate that the diagonal components of the stress tensor (i.e., the normal stress T_{zz} and the interfacial tension T_{xx} and T_{yy}) for a LJ(12,6)-type fluid (see Sec. IV A) constrained between smooth furrowed walls are strongly altered from their counterparts for the fluid between flat (planar) smooth walls. Note that by ''smooth'' we mean that the walls lack structure on the molecular scale, which is a reasonable approximation in case fluid molecules are much larger than substrate atoms. The furrowed walls, however, possess nanoscopic structure in the normal (z) direction and in one transverse (x) direction. The principal focus of our investigation is the effect of coupling between molecular and nanoscopic structures on the thermophysical properties of the film, and the smooth-wall approximation captures the effect.

The essential reason for the disparity between stress components of the film between furrowed and flat walls is the increase of order engendered by the confinement of the fluid molecules to the furrows, which constrain the packing of

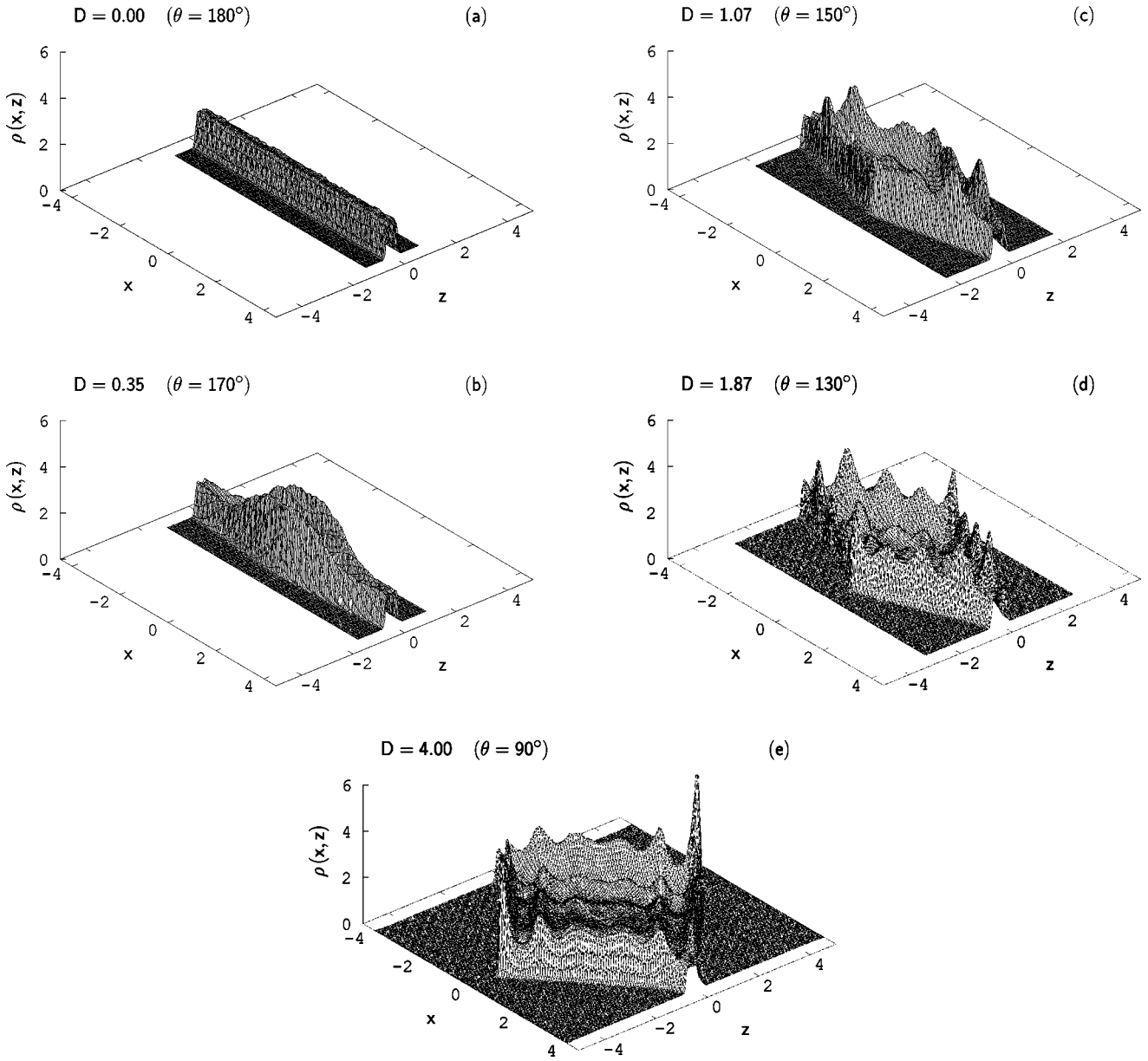

FIG. 4. Local density $\rho(x,z)$ for several furrow depths: (a) $D=0.00$ ($\theta=180°$), (b) $D=0.35$ ($\theta=170°$), (c) $D=1.07$ ($\theta=150°$), (d) $D=1.87$ ($\theta=130°$), and (e) $D=4.00$ ($\theta=90°$).

molecules in two dimensions, rather than in just one dimension, as for flat walls. A fluid molecule between smooth planar walls is subject to an ''external'' potential field that depends only on the distance (z) of the molecule from the substrates. As a result, the film orders itself in layers parallel with the walls, in a fashion analogous to the ordering of (spherical) molecules in the homogeneous fluid in spherical shells about a reference molecule. That is, the fluid between flat walls is ordered only in the direction normal to the walls. It is homogeneous in transverse (x,y) directions. Now with the introduction of furrows the film takes on additional order in the x direction, as the plots in Fig. 4 show. As the furrow deepens, the corner at the vertex sharpens. Fluid molecules therefore pack tightly in two transverse dimensions with respect to the corner. The fluid consequently takes on a solidlike order near the vertex. This is transmitted outward from the corner by epitaxy. Similar order was observed in the study of Schoen and Dietrich for a hard-sphere fluid confined

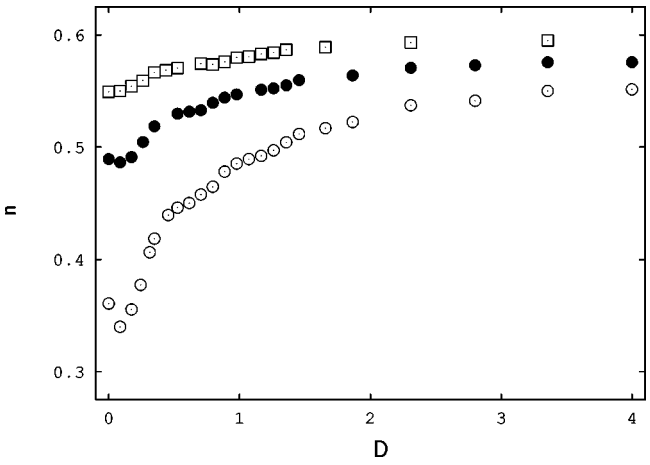

FIG. 5. Mean pore density n as a function of furrow depth for separations $s_z=2.0$ (○), 3.0 (●), and 4.0 (□).

between hard furrowed substrates and $\theta=90°$ [see Fig. 6(a) of Ref. [38]].

The dependence of the normal stress T_{zz} on the dihedral angle θ at fixed separation s_z, and vice versa, can be understood qualitatively by imagining the film to be partitioned into segments by planes parallel with the y-z plane. Speaking very roughly, we can express T_{zz} as a weighted average over the segments of T_{zz} for planar walls at a separation corresponding to the *mean* distance between the substrate surfaces of that segment. Shallow furrows are spanned by a few segments, which involve few points on the *planar* normal-stress curve. The values of T_{zz} at these few points add more or less constructively. On the other hand, deep furrows involve many segments over a broad range of separations and the corresponding planar T_{zz} values tend to cancel one another. Hence, as θ decreases over the range from 180° to 90°, the stress curve dampens toward the constant value of the bulk stress [see Fig. 2(c)].

A particularly noteworthy phenomenon is the strong, approximately linear, decrease of T_{xx} (i.e., the increase in tension of the film in the x direction relative to the bulk phase) with increasing depth D of the furrow at a fixed, relatively small, separation. We have argued that this is due to an increase in the order of the film in the x direction, and that it is analogous to the increase in tension in the z direction with increasing distance between *planar* (unfurrowed) walls, which is associated with the completion of a new layer in the film and a concomitant increase in order in the z direction. Since the film is always homogeneous in the y direction, variations in D influence T_{yy} much less than the other diagonal components. However, as pointed out in the discussion in Sec. V, variations of the structure of the film parallel with the cross section (i.e., parallel with the x-z plane) nevertheless affect T_{yy} appreciably.

Our results indicate the profound impact of coupling between molecular and nanoscopic scales on the thermophysical properties of geometrically constrained fluids, where the symmetry of the system is much reduced from that of the homogeneous fluid. We have explored the dependence of $T_{\alpha\alpha}$ on only two (s_z and D) of the *five* (T, μ, s_x, s_z, D) or *six* (if the x registry of the substrates is included) thermodynamic state variables that characterize this simple model. We would expect other properties, such as the shear stress and the phase behavior, to be similarly influenced.

ACKNOWLEDGMENTS

D.J.D. is thankful for the support of the Office of Naval Research, the U.S. National Science Foundation, and the Petroleum Research Fund administered by the American Chemical Society. M.S. is grateful for financial support from the Sonderforschungsbereich 448 ''Mesoskopisch strukturierte Verbundsysteme.'' We also acknowledge the Konrad-Zuse-Zentrum für Informationstechnik Berlin where computations were in part carried out.

APPENDIX A: DIFFERENTIATION OF THE CONFIGURATION INTEGRAL

To calculate the partial derivative of Z_N in Eq. (18), we transform to reduced dimensionless (primed) coordinates:

$$x_i'=\frac{x_i+s_x/2}{L+s_x/2},\qquad y_i'=\frac{y_i+s_y/2}{s_y/2},\qquad z_i'=\frac{z_i-z_1(x_i)}{\Delta z(x_i)}, \tag{A1}$$

where

$$\Delta z(x)=z_2(x)-z_1(x). \tag{A2}$$

The configuration integral can then be rewritten

$$Z_N=\prod_{i=1}^{N}\int_0^1 dx_i'\int_0^1 dy_i'\int_0^1 dz_i' J\exp(-U/k_BT), \tag{A3}$$

where the Jacobian of the transformation defined in Eqs. (A1) is given by

$$J=\left(L+\frac{s_x}{2}\right)^N s_y^N\prod_{k=1}^{N}\Delta z(x_k). \tag{A4}$$

From Eq. (A3) we obtain

$$\left(\frac{\partial Z_N}{\partial s_\alpha}\right)=\prod_{i=1}^{N}\int_0^1 dx_i'\int_0^1 dy_i'\int_0^1 dz_i'\left(\frac{\partial J}{\partial s_\alpha}-\frac{J}{k_BT}\frac{\partial U}{\partial s_\alpha}\right)\times\exp(-U/k_BT). \tag{A5}$$

We focus first on the case $s_\alpha=L$. Differentiation of the expression for J in Eq. (A4) yields

$$\frac{\partial J}{\partial L}=\frac{NJ}{L+s_x/2}\left[1+\frac{1}{N}\sum_{k=1}^{N}\left(x_k+\frac{s_x}{2}\right)\frac{\Delta z'(x_k)}{\Delta z(x_k)}\right], \tag{A6}$$

where $\Delta z'\equiv d\Delta z/dx$. From Fig. 1 it is clear that the ratio $\Delta z'/\Delta z$ depends on the domain of x. Using the equations of the planes of the substrate surfaces (see Fig. 1), we have

$$\frac{\Delta z(x)}{\Delta z'(x)}=\begin{cases}x+s_x/2+s_xs_z/4D, & -s_x/2\leqslant x\leqslant 0\\ x-s_x/2-s_xs_z/4D, & 0\leqslant x\leqslant s_x/2.\end{cases} \tag{A7}$$

From Eq. (17), we obtain

$$\frac{\partial U}{\partial L}=\frac{1}{2}\sum_{i=1}^{N}\sum_{j=1\neq i}^{N}u'(r_{ij})\frac{\partial r_{ij}}{\partial L}+\sum_{i=1}^{N}\frac{\partial\Phi(x_i,z_i)}{\partial L}, \tag{A8}$$

where $u'(r)\equiv du(r)/dr$. A long, painful sequence of manipulations eventually results in

$$\frac{\partial r_{ij}}{\partial L}=\frac{1}{r_{ij}(L+s_x/2)}\left\{x_{ij}^2+z_{ij}\left[z_i\left(x_i+\frac{s_x}{2}\right)\frac{\Delta z'(x_i)}{\Delta z(x_i)}-z_j\left(x_j+\frac{s_x}{2}\right)\frac{\Delta z'(x_j)}{\Delta z(x_j)}\right]\right\}. \tag{A9}$$

The partial derivative of Φ in Eq. (A8) can be expanded as

$$\frac{\partial\Phi(x_i,z_i)}{\partial L}=\frac{\partial\varphi_0(z_i)}{\partial L}+\frac{\partial\varphi_1(x_i,z_i)}{\partial L}$$

$$=\frac{\partial\varphi_0}{\partial z_i}\frac{\partial z_i}{\partial L}+\frac{\partial\varphi_1}{\partial x_i}\frac{\partial x_i}{\partial L}+\frac{\partial\varphi_1}{\partial z_i}\frac{\partial z_i}{\partial L}, \quad \text{(A10)}$$

where $\varphi_0(z)\equiv\varphi_0^{[1]}(z)+\varphi_0^{[2]}(z)$, $\varphi_1(x,z)\equiv\varphi_1^{[1]}(x,z)+\varphi_1^{[2]}(x,z)$, and [see Eqs. (A1)]

$$\frac{\partial x_i}{\partial L}=\frac{x_i+s_x/2}{L+s_x/2},$$

$$\frac{\partial z_i}{\partial L}=\frac{x_i+s_x/2}{L+s_x/2}\frac{\Delta z'(x_i)}{\Delta z(x_i)}z_i. \quad \text{(A11)}$$

APPENDIX B: FORMULAS FOR THE FLUID-SUBSTRATE FORCE

Here we derive formulas for the components of the mean-field force exerted by the substrates on fluid molecule i, $f_{n,\alpha}^{[k]}(x_i,z_i)=-\partial\varphi_n^{[k]}/\partial\alpha_i$, where $k=1,2$, $n=0,1$, and $\alpha=x,z$. We consider only the case $k=2$ since the components due to the lower substrate (1) can be expressed in terms of those due to the upper substrate (2). Differentiation of $\varphi_0^{[2]}(z_i)$ given in Eq. (5) with respect to z_i yields

$$f_{0,z}^{[2]}(z_i)=-2\pi\epsilon\sigma^2\rho_s\left[\frac{2}{5}\left(\frac{\sigma}{s_z/2+D-z_i}\right)^{10}-\left(\frac{\sigma}{s_z/2+D-z_i}\right)^{4}\right]. \quad \text{(B1)}$$

From the relation $\varphi_0^{[1]}(z_i)=\varphi_0^{[2]}(-z_i)$, it follows that

$$f_{0,z}^{[1]}(z_i)=-f_{0,z}^{[2]}(-z_i). \quad \text{(B2)}$$

Differentiating $\varphi_1^{[2]}$ with respect to x_i and z_i, we obtain

$$f_{1,x}^{[2]}(x_i,z_i)=\frac{3\pi\epsilon\rho_s\sigma s_x D}{4}\sum_{m=-\infty}^{\infty}\int_0^1 d\tilde{z}'\tilde{z}'\times\left[\int_0^1 d\tilde{x}'\,\psi'(x_i'',z_i'')\frac{x_i''}{R}+\int_0^1 d\tilde{x}'\,\psi'(\hat{x}_i'',z_i'')\frac{\hat{x}_i''}{R}\right],$$

$$f_{1,z}^{[2]}(x_i,z_i)=\frac{3\pi\epsilon\rho_s\sigma s_x D}{4}\sum_{m=-\infty}^{\infty}\int_0^1 d\tilde{z}'\tilde{z}'\times\left[\int_0^1 d\tilde{x}'\,\psi'(x_i'',z_i'')\frac{z_i''}{R}+\int_0^1 d\tilde{x}'\,\psi'(\hat{x}_i'',z_i'')\frac{z_i''}{R}\right], \quad \text{(B3)}$$

where $\psi'=d\psi/dR$, with $R=\sqrt{x''^2+z''^2}$, is given by

$$\psi'=-\frac{1}{\sigma}\left[\frac{231}{32}\left(\frac{\sigma}{R}\right)^{12}-5\left(\frac{\sigma}{R}\right)^{6}\right]. \quad \text{(B4)}$$

From the symmetry restrictions $\varphi_1^{[1]}(x,z)=\varphi_1^{[2]}(x,-z)$ and $\varphi_1^{[k]}(-x,z)=\varphi_1^{[k]}(x,z)$, we deduce the following relations:

$$f_{1,x}^{[1]}(x_i,z_i)=f_{1,x}^{[2]}(x_i,-z_i),$$

$$f_{1,z}^{[1]}(x_i,z_i=-f_{1,z}^{[2]}(x_i,-z_i),$$

$$f_{1,x}^{[k]}(-x_i,z_i)=f_{1,x}^{[k]}(x_i,z_i), \quad \text{(B5)}$$

$$f_{1,z}^{[k]}(-x_i,z_i)=f_{1,z}^{[k]}(x_i,z_i).$$

The equalities in Eqs. (B2) and (B5) can be used to express the mean-field force due to the substrates at any point (x,z) in the central period in terms of the force components $f_x^{[2]}\equiv f_{1,x}^{[2]}$ and $f_z^{[2]}=f_{0,z}^{[2]}+f_{1,z}^{[2]}$ at the point $(|x|,|z|)$ in the large upper right quadrant. We follow the procedure outlined in Sec. IV for $\varphi^{[2]}$; that is, we store the force components on a rectangular grid prior to the GCEMC run, and interpolate to obtain the instantaneous off-grid values during the run.

[1] D. Beaglehole, J. Chem. Phys. **93**, 893 (1989).
[2] S. Garoff, E. B. Sirota, S. K. Sinha, and H. B. Stanley, J. Chem. Phys. **90**, 7505 (1989).
[3] I. M. Tidswell, T. A. Rabedeau, P. S. Pershan, and S. D. Kosowsky, Phys. Rev. Lett. **66**, 2108 (1991).
[4] P. S. Pershan, Ber. Bunsenges. Phys. Chem. **98**, 372 (1994).
[5] D. Andelman, J.-F. Joanny, and M. O. Robbins, Europhys. Lett. **7**, 731 (1988).
[6] M. O. Robbins, D. Andelman, and J.-F. Joanny, Phys. Rev. A **43**, 4344 (1991).
[7] J. L. Harden and D. Andelman, Langmuir **8**, 2547 (1992).
[8] R. R. Netz and D. Andelman, Phys. Rev. E **55**, 687 (1997).
[9] M. Sundarem, S. A. Chalmers, P. F. Hopkins, and A. C. Gossard, Science **254**, 1326 (1991).
[10] H. Rauscher, T. A. Jung, J.-L. Lin, A. Kirakosian, F. J. Himpsel, U. Rohr, and K. Küllen, Chem. Phys. Lett. **303**, 363 (1999).
[11] B. F. Jones and F. Galan, *Reviews in Mineralogy, Vol. 19: Hydrous Phyllosilicates* (Bookcrafters, Chelsea, 1988).
[12] J. A. Mann, Jr., L. Romero, R. R. Rye, and F. G. Yost, Phys. Rev. E **52**, 3967 (1995).
[13] R. R. Rye, F. G. Yost, and J. A. Mann, Langmuir **12**, 4625 (1996).
[14] R. R. Rye, F. G. Yost, and J. A. Mann, Langmuir **12**, 555 (1996).
[15] J. B. Knight, A. Vishwanath, J. P. Brody, and R. H. Austin, Phys. Rev. Lett. **80**, 3863 (1998).
[16] M. Grunze, Science **283**, 41 (1999).
[17] S. Dietrich, in *Proceedings of the NATO-ASI ''New Approaches to Old and New Problems in Liquid State Theory—Inhomogeneities and Phase Separation in Simple, Complex, and Quantum Fluids,'' held at Patti Marina (Messina), July*

7–17, 1998, edited by C. Caccamo (Kluwer, Dordrecht, 1999), p. 197.
[18] P. Lenz and R. Lipowsky, Phys. Rev. Lett. **80**, 1920 (1997).
[19] H. Gau, S. Herminghaus, P. Lenz, and R. Lipowsky, Science **283**, 46 (1999).
[20] P. Swain and R. Lipowsky, Langmuir **14**, 6772 (1998).
[21] P. Swain and R. Lipowsky, Europhys. Lett. **49**, 203 (2000).
[22] W. Koch, S. Dietrich, and M. Napiórkowski, Phys. Rev. E **51**, 3300 (1995).
[23] C. Bauer and S. Dietrich, Phys. Rev. E **60**, 6919 (1999).
[24] L. J. Douglas Frink and A. G. Salinger, J. Chem. Phys. **110**, 5969 (1999).
[25] C. Chmiel, K. Karykowski, A. Patrykiejew, W. Ryzsko, and S. Sokolowski, Mol. Phys. **81**, 691 (1994).
[26] P. Röcken and P. Tarazona, J. Chem. Phys. **105**, 2034 (1996).
[27] P. Röcken, A. Somoza, P. Tarazona, and G. H. Findenegg, J. Chem. Phys. **108**, 8689 (1998).
[28] M. Schoen and D. J. Diestler, Chem. Phys. Lett. **270**, 330 (1997).
[29] M. Schoen and D. J. Diestler, Phys. Rev. E **56**, 4427 (1997).
[30] H. Bock and M. Schoen, Phys. Rev. E **59**, 4122 (1999).
[31] H. Bock and M. Schoen, J. Phys.: Condens. Matter **12**, 1545 (2000).
[32] H. Bock and M. Schoen, J. Phys.: Condens. Matter **12**, 1569 (2000).
[33] L. D. Gelb, K. E. Gubbins, R. Radhakrishnan, and M. Sliwinska-Bartkowiak, Rep. Prog. Phys. **62**, 1573 (1999).
[34] M. Borówko and A. Patrykiejew, in *Computational Methods in Colloid and Interface Science*, edited by M. Borówko (Dekker, New York, 2000), p. 245.
[35] J. E. Curry, F. Zhang, J. H. Cushman, M. Schoen, and D. J. Diestler, J. Chem. Phys. **101**, 10 824 (1994).
[36] M. Schoen, J. H. Cushman, and D. J. Diestler, J. Chem. Phys. **87**, 5464 (1987).
[37] C. L. Rhykerd, Jr., M. Schoen, D. J. Diestler, and J. H. Cushman, Nature (London) **330**, 461 (1987).
[38] M. Schoen and S. Dietrich, Phys. Rev. E **56**, 499 (1997).
[39] D. Henderson, S. Sokolowski, and D. Wasan, Phys. Rev. E **57**, 5539 (1998).
[40] K. Rejmer, S. Dietrich, and M. Napiórkowski, Phys. Rev. E **60**, 4027 (1999).
[41] A. O. Parry, C. Rascón, and A. J. Wood, Phys. Rev. Lett. **83**, 5535 (1999).
[42] A. O. Parry, C. Rascón, and A. J. Wood, preprint, cond-mat/9911431.
[43] M. Plischke and B. Bergersen, *Equilibrium Statistical Physics*, 2nd ed. (World Scientific, Singapore, 1994), Chap. 2.3.
[44] D. J. Adams, Mol. Phys. **28**, 1241 (1974).
[45] M. Schoen, in *Computational Methods in Colloid and Interface Science* (Ref. [34]), p. 1.
[46] N. Metropolis, A. W. Rosenbluth, M. N. Rosenbluth, A. H. Teller, and E. Teller, J. Chem. Phys. **21**, 1087 (1953).
[47] W. W. Wood, in *Proceedings of the International School of Physics ''Enrico Fermi,''* edited by G. Ciccotti and W. G. Hoover (North-Holland, Amsterdam, 1986), p. 3.
[48] M. P. Allen, in *Monte Carlo and Molecular Dynamics of Condensed Matter Systems*, edited by K. Binder and G. Ciccotti (Bologna, Società Italiana di Fisica, 1996), Vol. 49, p. 255.
[49] N. B. Wilding and M. Schoen, Phys. Rev. E **60**, 1081 (1999).
[50] M. P. Allen and D. J. Tildesley, *Computer Simulation of Liquids* (Clarendon, Oxford, 1987).